Nuclear Instruments and Methods in Physics Research A 621 (2010) 424–430

Contents lists available at ScienceDirect

Nuclear Instruments and Methods in Physics Research A

journal homepage: www.elsevier.com/locate/nima

Variation of electric shielding on virtual Frisch-grid detectors

J.K. Polack [a,b], M. Hirt [a,b], J. Sturgess [a,b], N.D. Sferrazza [a], A.E. Bolotnikov [a,*], S. Babalola [a,c], G.S. Camarda [a], Y. Cui [a], S.U. Egarievwe [d], P.M. Fochuk [e], R. Gul [a], A. Hossain [a], K. Kim [a], O.V. Kopach [e], L. Marchini [a,f], G. Yang [a], L. Xu [a], R.B. James [a]

[a] 197-D, Brookhaven National Laboratory, Upton, NY, USA
[b] University of Michigan, Ann Arbor, MI, USA
[c] Fisk University, Nashville, TN, USA
[d] Alabama A&M University, Normal, AL, USA
[e] Chernivtsi National University, Chernivtsi, Ukraine
[f] IMEM-CNR, Parma, Italy

ARTICLE INFO

Article history:
Received 24 December 2009
Received in revised form
11 May 2010
Accepted 16 May 2010
Available online 24 May 2010

Keywords:
CdZnTe
Virtual Frisch-grid detectors
Gamma-ray detectors

ABSTRACT

Because of the low mobility of holes, CdZnTe (CZT) detectors operate as electron-transport-only type devices whose particular geometrical parameters and contacts configurations are specially chosen to minimize the contribution of uncollected holes into the output signal amplitudes (induction effect). Several detector configurations have been proposed to address this problem. One of them employs a large geometrical aspect ratio, parallelepiped-shaped crystal with two planar contacts on the top and bottom surfaces (anode and cathode) and an additional shielding electrode placed on a crystal's side to create the virtual Frisch-grid effect. We studied the effect of the shielding electrode length, as well as its location, on the responses of $6\times6\times15$ mm^3 virtual Frisch-grid detectors. We found that the length of the shielding electrode placed next to the anode can be reduced to 5 mm with no adverse effects on the device performance. Meanwhile, this allows for charge loss correction by reading the cathode signals.

Published by Elsevier B.V.

1. Introduction

CdZnTe (CZT) is a promising semiconductor material for ambient temperature gamma-ray detectors [1]. However, since CZT detectors operate as electron-transport-only devices their particular geometrical parameters and contacts should be specially chosen to minimize the contribution of uncollected holes into the output signal amplitudes (called the induction effect). Several detector configurations have been proposed to address this problem: one of them employs a large geometrical aspect ratio, parallelepiped-shaped (bar) crystal with two planar contacts (anode and cathode) and an additional shielding electrode placed on a crystal's sides to create the virtual Frisch-grid effect [2–4]. The arrays of such detectors offer a robust and inexpensive approach for making large-area instruments for imaging and spectroscopy of gamma rays [5–6]. Such arrays potentially can replace the large-volume but more expensive single 3D detectors in applications with slightly relaxed requirements to position- and energy-resolution. Although the 3D detector approach represents more advanced technology in CZT detectors, today, it is not practical for making large-volume imaging instruments because of the high cost and low availability of big CZT crystals, such as the $20\times20\times15$ mm^3 used in 3D detectors. In contrast, thick, up to 20 mm, but small cross-sectional area, $\sim6\times6$ mm^2, virtual Frisch-grid detectors can be fabricated from relatively thin, 7 mm, CZT wafers. This provides greater flexibility in cutting and facilitates more detailed screening for defects before making actual devices. Small 4×4 arrays consisting of 16 bars can also offer advantages as gamma-ray spectrometers in compact, hand-held devices that combine an excellent energy resolution of $<1.5\%$ at 662 keV and high detection efficiency and can be manufactured at a much lower cost. The effective area of the 4×4 array of $6\times6\times15$ mm^3 detectors is equivalent to the area of the largest 3D detector available today.

The design of a virtual Frisch-grid detector relies on using a large geometrical aspect ratio, parallelepiped-shaped (bar) crystal with the cathode and anode electrodes deposited on the top and bottom surfaces and an additional shielding electrode placed on a crystal's side to create the virtual Frisch-grid effect. Such devices are fabricated by wrapping or coating the sides of a crystal with a thin layer of an insulating film followed by a layer of aluminum or copper foil. To achieve the strongest efficient shielding effect, the side electrode must be extended to cover the entire length of

* Corresponding author. Tel.: +1 631 344 8014; fax: +1 631 344 3374.
E-mail address: bolotnik@bnl.gov (A.E. Bolotnikov).

0168-9002/$ - see front matter Published by Elsevier B.V.
doi:10.1016/j.nima.2010.05.035

the crystal. However, if such detectors are used in an array with electronic correction of charge loss, the shield must be shortened so the cathode becomes sensitive to the interaction events taking place inside the whole detector's volume, even close to the anode. Using long CZT crystals with a high geometrical aspect ratio is a key requirement for achieving the high energy resolution and high peak-to-Compton ratio. However, in these thick devices, the electron drift times exceed 1 μs. Due to these relatively long drift times, the charge trapping due to defects becomes more severe and needs to be corrected to retain high spectral resolution expected from CZT. This can be achieved by implementing the cathode readout scheme, which would allow us firstly to correct electron trapping and secondly to reject the events interacting near the anode which contribute to the background.

There are contradicting requirements in this approach. To ensure strong shielding effect of the virtual Frisch-grid, the side electrode should cover the entire area of the device's surface. But when the entire detector is shielded, very few signals can be detected by the cathode. This makes the cathode insensitive to the events interacting deep inside the detector. On the other hand, it is critical for the electronic correction to be able to detect events by both the anode and the cathode. Using long detectors should solve this problem, since a wide area near the cathode can be left uncovered by metal without lowering the effectiveness of shielding the anode. Furthermore, by assembling the arrays in which the cathodes of several detectors, e.g., 4×4 modules, are connected together the shielding effect will be enhanced. This design should efficiently shield the anode whilst allowing us to readout the cathode signals required for correcting the charge losses due to electron trapping.

The goal of our work was to validate this new approach for design of virtual Frisch-grid detector arrays with a common cathode and demonstrate its feasibility to improve the energy resolution and peak-to-Compton ratio of long, >15 mm, devices.

2. Experimental setup

Over 20 $6\times6\times15\ mm^3$ virtual Frisch-grid detectors with good spectral responses were selected for these studies: the pulse-height spectra taken for these detectors indicated uniform charge collection over the entire crystals' volumes, while energy resolutions were found to be $\sim$2% FWHM at 662 keV with a loss of resolution that could be entirely attributed to the electron trapping effect. These measurements were completed with the detectors having been fabricated based on our previous design [5,6] in which the shielding electrode is disconnected from the cathode, and covered the full length of the detector. A high-voltage bias (with respect to the anode) was applied to the cathode, while the shielding and anode electrodes were kept at the same (ground) potential, a feature that is important in assembling arrays of such detectors. To insulate the CZT surface from the shield, the crystals were encapsulated in an ultra-thin polyester shrink tube [5]. Fig. 1(a) depicts the encapsulated crystal in a 100 μm-thin polyester shell detector with a $\sim$5 mm wide shielding electrode.

Several measurements were made for each crystal with varying shield lengths ranging between 3 and 15 mm, which covered nearly the entire detector. For each shielding electrode configuration, a pulse-height spectrum was collected using an uncollimated ^{137}Cs source placed $\sim$1 cm above the cathode. Time-resolved measurements were also taken by adding a 1-in^3 BaF_2 detector to our experimental setup located approximately 3 in. above our CZT housing as schematically shown in Fig. 1(b). To take these measurements, we used a ^{68}Ge source collimated by a customized tungsten housing, which only allowed photons to be emitted in the directions of the detectors. The ^{68}Ge source emits pairs of back-to-back 511 keV photons due to positron annihilation that were used to produce coincidence signals in the CZT and BaF_2 detectors. The fast signals generated in the BaF_2 detector were used to determine the time of birth for the interaction events inside CZT detector. We tested the detector by placing it inside a special holder with two BNC connectors as illustrated in Fig. 1(c). This arrangement allowed us to apply a high-voltage bias on the cathode and to read the signals from both the cathode and the anode.

We employed a LeCroy Waverunner to digitize and record the output signals (waveforms) from the eV-Product charge-sensitive preamplifiers (eV-5093). We used a qualify trigger, meaning that an event is accepted when an anode signal above a certain threshold arrives within 2 μs after a signal from the photomultiplier tube (PMT). We applied a digital-pulse analysis described elsewhere [7] to evaluate the dependencies of the signals' amplitudes versus the electrons' drift times. Due to the system's large stray capacitors and long cables, the contribution electronic noise to the peak widths was 4–5 keV FWHM. As an example, Fig. 2(a) shows typical coincidence signals from the cathode, anode and PMT as captured by the Waverunner. As expected, the beginning of the cathode signal coincides with the PMT's trigger signal, which means that the cathode signal can be used to evaluate the electron drift time. The anode signal appears to be delayed due to the anode shielding effect. The horizontal dashed lines represent thresholds setup for the cathode and PMT signals during the measurements, while the vertical ones indicate a moment of 511 keV photon interaction (left) and the arrival time of an electron cloud at the anode (right). The difference between these two moments gives the total drift time. The amplitudes of the anode and cathode signals were evaluated by averaging the corresponding top, flat portion of the pulses over $\sim$500 ns after the baseline subtraction [7]. A set of at least 20,000 coincidence interaction waveforms was gathered for each shielding electrode configuration and used to evaluate changes in the device's performance. These data were used to plot the dependence on the amplitudes of the output signals measured from the anode and cathode versus the drift time (or interaction depth) that we termed the correlation curve. Such dependencies provide the full information about performances of CZT detectors and can be evaluated theoretically. As an example, Fig. 2(b) shows the dependence of the anode signal versus the drift time modeled for a $6\times6\times15\ mm^3$ virtual Frisch device with the shielding electrode covering the full length of the crystal. This is a special case for which the calculation of the weighting potential can be done analytically [8]. In the model we assume a uniform distribution of interaction points over the device volume and no charge loss due to electron trapping. A 2000 V bias was assumed to be applied. Each dot in this plot represents an individual interaction event. The upper boundary of the dots continuum in Fig. 2(b) corresponds to interaction close to the side edges of the detector where the shielding effect is strongest, while the dots near the lower boundary represent the events taking place along the middle axis of the device. The important feature of the distribution is that it converges into a straight horizontal line at a distance of $\sim$1/3 of the crystal length above the anode indicating a 100% shielding efficiency in this region of the device. If the length of the side electrode is shortened, this would reduce the shielding efficiency near the cathode and force the lower boundary of the dots continuum to move down making its average slope more positive. In contrast, taking into account the charge trapping effect would result in negative slope of the converged distribution. In reality, both the effects compensate each other.

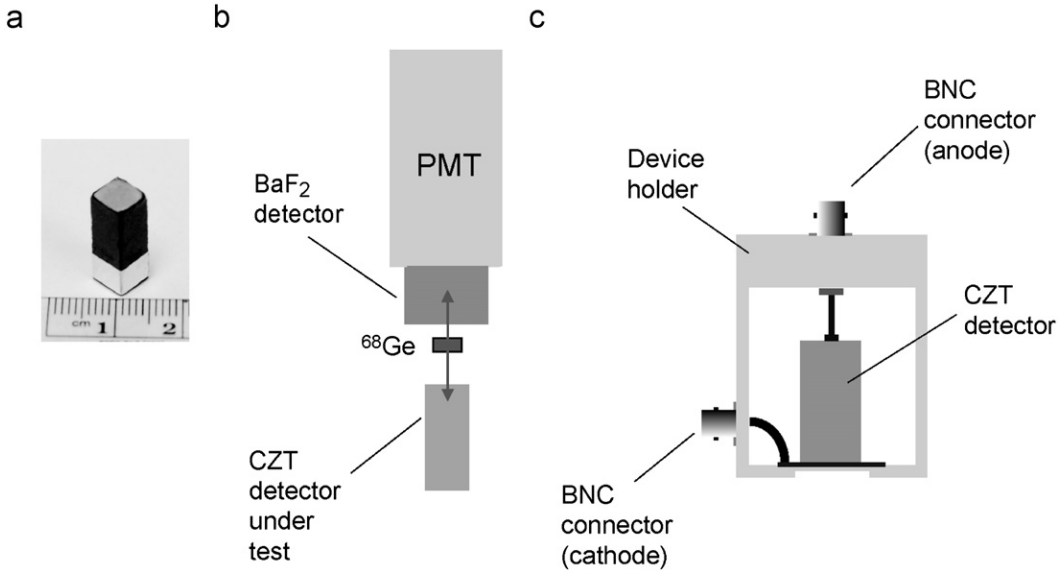

Fig. 1. (a) $6 \times 6 \times 15$ cm^3 virtual Frisch-grid detector encapsulated in a 100-μm-thin shell polyester with a 5-mm wide shielding electrode. (b) The experimental setup used to measure coincidence signals between the fast BaF_2 scintillation detector and CdZnTe detector under the tests. (c) Schematic of the device holder with two BNC connectors.

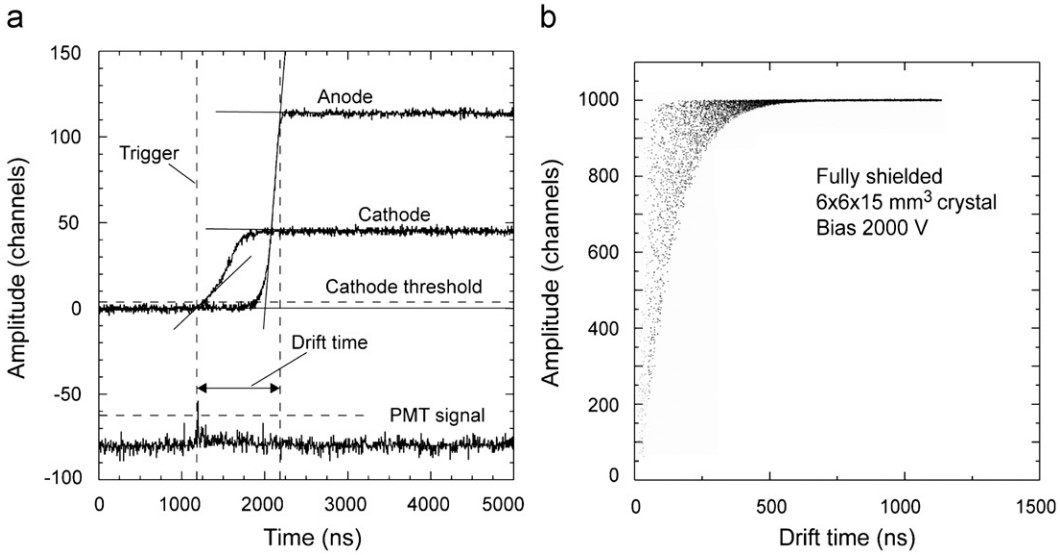

Fig. 2. (a) The typical coincidence signals captured from the cathode, anode and PMT. The horizontal dashed lines define thresholds for the cathode and PMT signals, while the vertical ones define the interaction time (left) and electron arrival time at the anode (right). The drift time is determined as a time interval between these two moments. (b) The dependence on the anode signal versus the drift time calculated for a $6 \times 6 \times 15$ mm^3 fully shielded virtual Frisch-grid detector assuming a uniform distribution of interaction points over the device volume and a 2000 V cathode bias.

3. Results and discussion

Fig. 3 shows the correlations between the output signals and the drift times (or interaction depths) evaluated for a $6 \times 6 \times 15$ mm^3 detector with different shield lengths (measured from the anode side) starting from none to 10-mm long as indicated on the plots. The cathode bias is 2000 V. In this paper, we presented the results from testing a single detector. However, all detectors gave similar results. As seen, the photoabsorption events concentrate along lines that represent the correlations between the amplitudes of charge signals and the drift times (or the interaction depths). The plots in column (a) show the correlations between the anode signals and drift times evaluated for all triggered events, while the plots in column (b) show only those events when the cathode signals were also detected (the cathode signals rose above the threshold level). We set the threshold for the cathode signals just above the noise level. As seen, for the fully unshielded detector (top) the correlation curves in (a)- and (b)-plots are almost identical as expected from the symmetrical device. However, when the shield length is progressively increased, we see that many events in the (a)-plots interacting close to the anode are missing from the (b)-plots, indicating that the cathode is not sensitive to the events interacting deep inside the crystals in shielded detectors. This is also reflected in the plots in column (c), which contain the correlations between the cathode signals and drift times. Again, in the case of fully unshielded detector the distribution of the anode signals is nearly identical to the cathode one. As the shield's

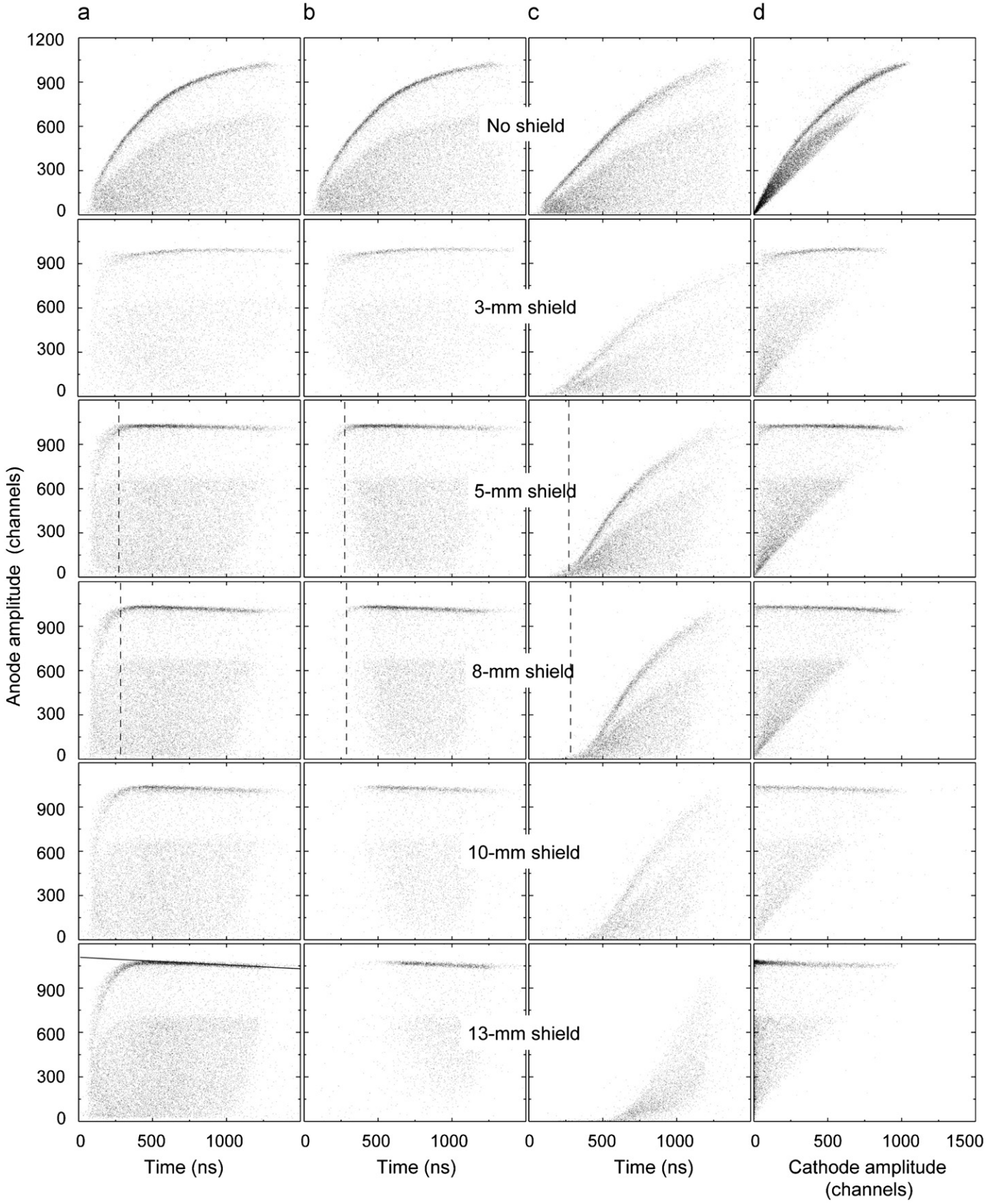

Fig. 3. Correlation curves measured for $6 \times 6 \times 15\ \mathrm{mm}^3$ virtual Frisch-grid detector with different widths of the shielding electrode measured from the anode level indicated in the plots: (a) the correlations between the anode signals and drift times evaluated for all triggered events; (b) same as (a) but shows only those events when the cathode signals were also detected (the cathode signals rose above the threshold level); (c) the correlations between the cathode signals and drift times; (d) the correlations between the anode and cathode signals. The cathode bias is 2000 V; the electron lifetime evaluated by measuring the slope of the correlation curve in the case of 13-mm shield was found to be $\sim 20\ \mu\mathrm{s}$.

length increases, the left edge of the cathode signals plateau shifts towards the longer drift times indicating that the cathode does not sense the events interacting deep inside the crystals near the anode (short drift times mean interactions points are located close to the anode). In fact, the position of the left edge determines a geometrical boundary in the detector (measured from the anode) below which the events cannot be detected by the cathode. For the nearly fully shielded detector (13 mm), the cathode sensitive area shrinks down to ~7-mm region near the cathode. Due to constraints of our experimental setup, we did not take measurements for the fully shielded detector. However, the calculations, which can be done analytically in this case, predict that the sensitive area decreases down to ~5 mm.

The plots in Fig. 3 allow us to find the optimal range of the shield lengths that increases the cathode's sensitivity comparison to the fully shielded detector and, at the same time, does not affect the device response due to the less efficient shielding. As is evident from comparing the (a) and (b) plots, when the shielding electrode covers 5–8 mm of the detector's length, the cathode detects nearly all events, except for those interacting very close to the anode, i.e., in the region between the virtual Frisch-grid and the anode that contributes to the background, and should be rejected anyway. In the anode signal distributions (a) this region corresponds to the short drift times, below the point at which the correlation curves start sharply decreasing (marked by dashed lines in the 5- and 8-mm shield length plots). In contrast, using

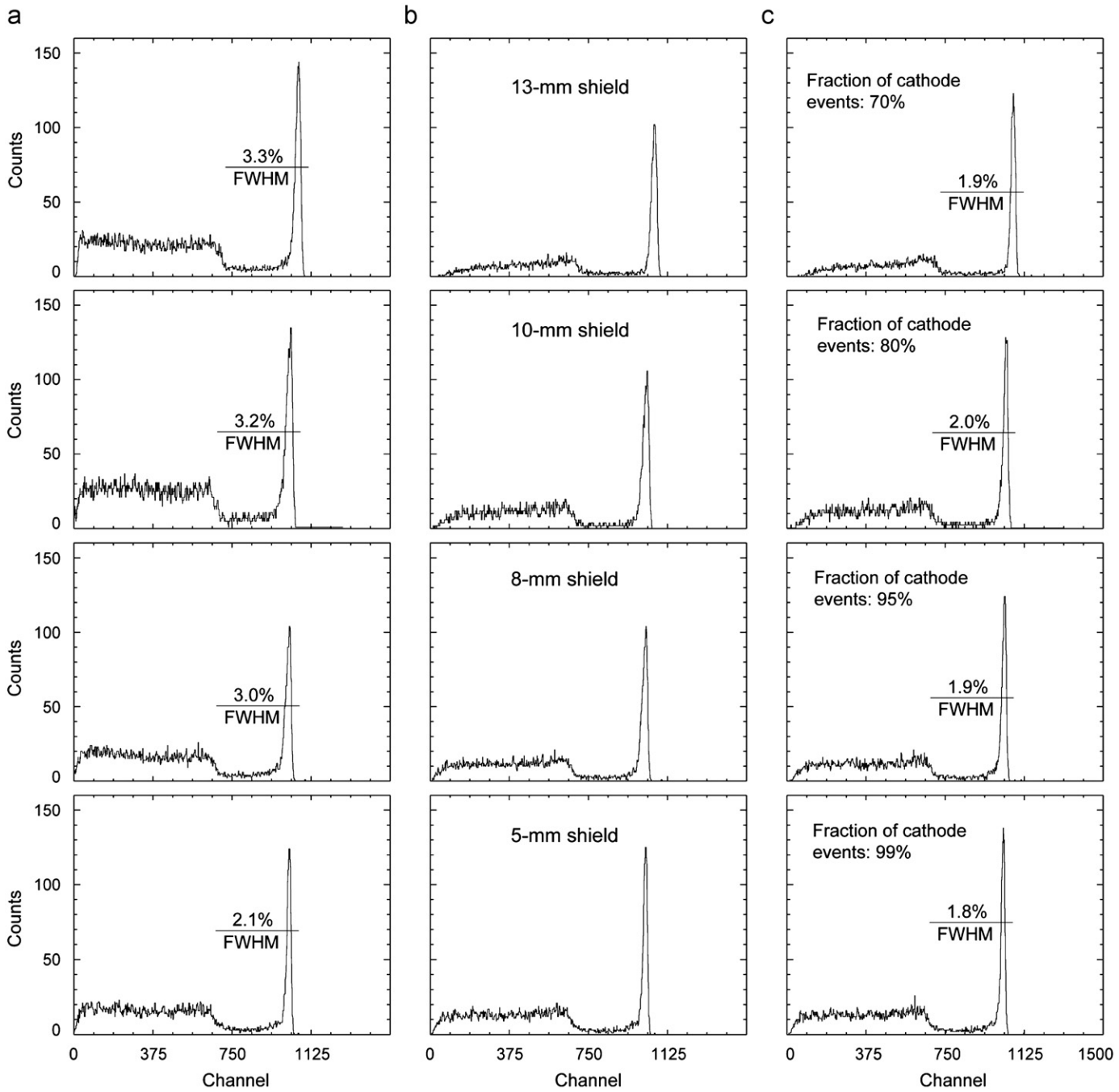

Fig. 4. Pulse-height spectra obtained by histograming corresponding to the distributions shown in Fig. 3: column (a) shows spectra evaluated for all triggered events; columns (b) and (c) contain only those events when the cathode signals rise above the threshold (one sigma of the electronic noise); columns (b) and (c) represent spectra before and after charge loss correction.

10- or 13-mm shields would result in too many missed events and consequently, a decrease in detection efficiency.

Another factor to consider when selecting the optimal length of the shielding electrode is the slope of the curve in the anode signal distributions (a). For the fully (or nearly fully like in the case of 13-mm shield) shielded detector, the slope of the correlation curve is determined only by electron trapping because, as followed from the simulations, the weighting potential remains constant at least for half of the device. In this case, the slope of the correlation curve (solid line in the plot of column (a) for the case of the 13-mm shield) can be used to evaluate the electron lifetime τ. Fitting the slopes measured for the detectors used in these measurements, we found that $\tau \sim 15$–30 μs. In a general case, the slope is determined by changes of the weighting potential inside the device, and electron loss due to trapping. Except for the region near the anode, these two effects, approximated by linear functions with opposite slopes, compensate for each other. For example, in the 5-mm shield case, the correlation curve becomes almost flat signifying that no electronic correction is required in this case. However, this is not a convenient and well controllable way to correct for the electron loss because it would depend on the CZT material properties ($\mu\tau$ product) and the applied bias. If the length is too short, as in the case of the 3-mm shield, the correlation curve has two slopes which will be difficult to correct electronically. It is clear that the length of the shield should be long enough to ensure a slightly negative slope of the correlation curve so that the detector response could be electronically corrected by reading signals from the cathode. It is worth mentioning that both the amplitude and the drift time evaluated from the cathode signals correlate to the anode signals, as illustrated in the (b) and (d)plots, and can be used to implement the charge loss corrections.

The plots in Fig. 3 prove that by reducing the size of the shielding electrode down to ~1/3 of the detector's length enables the cathode to detect the events interacting deep inside the crystals and, at the same time, does not affect the photopeak efficiency. This is also illustrated in Fig. 4, which contains the pulse-height spectra corresponding to the distributions in Fig. 3. The plots in column (a) show the spectra evaluated for all triggered events, while the spectra in columns (b) and (c) contain only those events when the cathode signals rise above one sigma of the electronic noise (10 channels on a plot's scale). The difference between columns (b) and (c) is that they represent spectra before and after applying correction for charge trapping. The peak widths (% FWHM at 551 keV) in the corrected spectra in the range 1.8–2.0% are primarily governed by the electronic noise. In contrast, the peak widths in the uncorrected spectra improve from 3.3% to 2.1% when the length of the shielding electrode decreases between 13 and 5 mm, indicating the compensation effect for the charge loss due to electron trapping. Column (c) also contains fractions (%) of the photopeak events detected by the cathode to the total number of the anode events. As seen, when the length of the shielding electrode is reduced below 8 mm almost all photopeak events are seen by the cathode.

Fig. 5 shows the ^{137}Cs and ^{133}Ba pulse-height spectra measured from a detector with the reduced shielding electrode whose size and location was optimized to achieve the best performance. It demonstrates that correcting the electron trapping by optimizing the shielding effect of the virtual Frisch-grid achieves a noise-subtracted energy resolution of $<1\%$ FWHM at

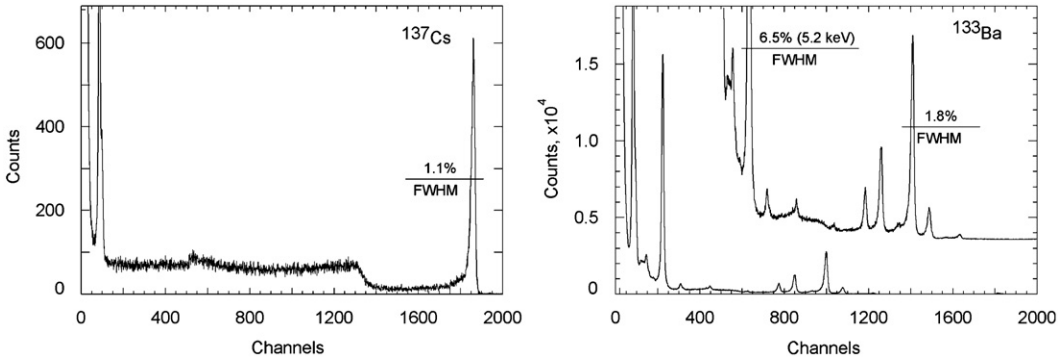

Fig. 5. The representative pulse-height spectra of ^{137}Cs and ^{133}Ba pulse-height spectra measured from the detector with the reduced shielding electrode the width of which was optimized to achieve the best performance. We used standard spectroscopy electronics with a shaping time of 2 μs for these measurements. The electronic noise was equivalent to ~4 keV FWHM.

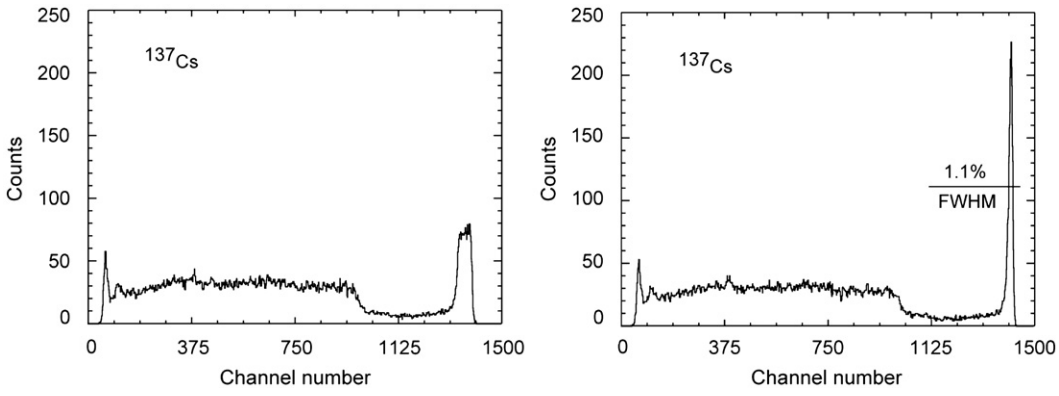

Fig. 6. Application of charge-loss correction by reading the cathode signals: ^{137}Cs spectrum before (left), and after (right) charge-loss correction. Energy resolution improved from ~3.7% down to 1.1% FWHM.

662 keV for a detector of $6 \times 6\,mm^2$ cross-sectional area and 15 mm long. To obtain these measurements, we used standard spectroscopy electronics with a shaping time of 2 μs. The electronic noise was equivalent to ~4 keV FWHM. We note that adjusting the size and location of the shielding electrode for each detector (which also depends on the applied bias) would be too unreliable, complex, and cumbersome. In addition, it inevitably would increase the thickness of the poorly shielded regions near the anode. Hence, the best, most robust approach for this type of device was to use the same electrode, i.e., identical width shield for all detectors placed near the anode and to employ the drift time correction technique.

Fig. 6 depicts an example of applying the charge-loss correction by reading the cathode signals without triggers. Here, the detector, with its 5.5 mm wide shielding electrode, was illuminated by photons from the uncollimated ^{137}Cs source. We collected the ^{137}Cs spectrum, left, before charge-loss correction, and, right, after including it. This correction yielded a much-improved energy resolution from ~3.7% down to 1.1% FWHM, which is excellent for a 15 mm long crystal. Both the spectra contain events for which cathode signals were detected. The corrected resolution is slightly larger than that obtained via shield adjustment because of the additional electronic noise that we were unable to minimize with digital pulse-shape analysis.

4. Conclusions

Virtual Frisch-grid detector arrays represent a promising approach for making large-area instruments for imaging and spectroscopy of gamma rays. Such arrays can be a substitute for the large-volume 3D detectors in applications with relaxed requirements to position- and energy-resolution. The main advantage of the bar-shaped virtual Frisch-grid detectors is that they use small cross-sectional area $\sim 6 \times 6\,mm^2$ but very long > 15 mm CZT crystals that can be fabricated from relatively thin, 7 mm, CZT wafers. This allows for larger flexibility in cutting and screening for defects before making devices.

On the other hand, use of long CZT detectors requires signal correction to ensure high-energy resolutions offered by these types of devices. The charge-loss correction technique relies on using the signals readout from the cathode, which raises a question regarding the optimal length of the shielding electrode used to produce virtual Frisch-grid effect. The optimal shielding electrode should provide a strong shielding effect for the majority of the device volume and, at the same time, ensure that the cathode will be sensitive to the events interacting deep inside the detector.

We demonstrated that the length of the shielding electrode in long, > 15 mm, virtual Frisch-grid detectors can be reduced down to 3 mm without lowering the effectiveness of shielding the anode. Furthermore, by assembling the arrays in which the cathodes of several detectors, e.g., 4×4 modules, are connected together, the shielding effect will be enhanced. This design should efficiently shield the anode whilst letting us to readout the cathode signals for correcting the charge loss due to trapping.

However, the length of the shielding electrode cannot be too short, because the reduction in the shielding efficiency would eventually over-compensate the effect of the charge loss and deteriorate the device's energy resolution. Moreover, to minimize the thickness of the poorly shielded layer near the anode, the shielding electrode should be close to it. The optimal length depends on material properties ($\mu\tau$ product) and the applied bias. We found this length to be approximately 5–6 mm for the $6 \times 6 \times 15\,mm^3$ detectors we studied.

Acknowledgments

This work was supported by US Department of Energy, Office of Nonproliferation Research and Development, NA-22. The manuscript has been authored by Brookhaven Science Associates, LLC under Contract no. DE-AC02-98CH1-886 with the US Department of Energy. The United States Government retains, and the publisher, by accepting the article for publication, acknowledges, a world-wide license to publish or reproduce the published form of this manuscript, or allow others to do so, for the United States Government purposes.

References

[1] G. Knoll, in: Radiation Detection and Measurement, 3rd ed., Wiley, New York, 2000.
[2] D.S. McGregor, R.A. Rojeski, U.S. Patent 6,175,120, issued January 6, 2001.
[3] G. Montémont, M. Arques, L. Verger, J. Rustique, IEEE Trans. Nucl. Sci. NS-48 (2001) 278.
[4] Alireza Kargar, Adam C. Brooks, Mark J. Harrison, Kyle T. Kohman, Rans B. Lowell, Roger C. Keyes, Henry Chen, Glenn Bindley, Douglas S. McGregor, IEEE Trans. Nucl. Sci. NS-56 (3) (2009) 824.
[5] A.E. Bolotnikov, G.C. Camarda, G.A. Carini, M. Fiederle, L. Li, D.S. McGregor, W. McNeil, G.W. Wright, R.B. James, IEEE Trans. Nucl. Sci. NS-53 (2) (2006) 607.
[6] A.E. Bolotnikov, G.S. Camarda, Y. Cui, K.T. Kohman, L. Li, M.B. Salomon, R.B. James, IEEE Trans. Nucl. Sci. NS-54 (2007) 821.
[7] A.E. Bolotnikov, G.S. Camarda, G.A. Carini, M. Fiederle, L. Li, G.W. Wright, R.B. James, Performance studies of CdZnTe detector by using a pulse-shape analysis, in: Proceedings of the SPIE, Hard X-Ray and Gamma-Ray Detector Physics VII, Bellingham, WA, 2005, SPIE, 59200K-1, 59200K-12.
[8] N.N. Lebedev, I.P. Skalskay, J.S. Ufland, Collection of Mathematical Physics Problems, 1955.